ADVANCED PHOTONICS RESEARCH
Open Access
www.adpr-journal.com

Estimating the Optically Pumped Threshold Fluence of Thin-Film Gain Media Using Arbitrary Excitation Beams

Nirav Annavarapu, Iakov Goldberg, Karim Elkhouly, Sarah Hamdad, Jan Genoe, Robert Gehlhaar, and Paul Heremans**

Optically pumped threshold fluences are a widely reported metric to benchmark the performance of thin-film gain media and lasers. Estimating the threshold fluence for nonhomogeneous beams, such as a circular Gaussian excitation, is not trivial since the average fluence depends on the estimated spot diameter. Using an exemplary lead halide perovskite film, the inversion volume at different pump energies is mapped. It is shown that the peak fluence of an arbitrary spatial beam profile is more relevant at the threshold, as it provides an upper bound to the threshold fluence. Also, simple conversion factors to estimate the peak fluence using Gaussian excitation beams are provided and the methodology to arbitrary profiles is extrapolated. Furthermore, it is advocated for using flat-top or uniform stripe excitations to unambiguously extract the threshold fluence, since these excitations display minor discrepancies between the average and peak fluence, and keep the inversion volume relatively constant during the measurement.

1. Introduction

In recent decades, various material systems such as lead halide perovskites, colloidal quantum dots, and organic semiconductors have gained prominence as potential gain media for thin-film laser diodes.[1–3] These materials can be deposited using ambient temperature processing methods and can be engineered to emit light in the visible and infrared spectral ranges.[4–6] Photoluminescence (PL) and amplified spontaneous emission (ASE) are consistently observed when these materials are excited by high-intensity optical sources.[7–10] Subsequently, numerous demonstrations of optically excited lasing have been reported,[9,11–16] and considerable research efforts have been directed toward achieving electrically pumped ASE and lasing from these systems.[17–20]

Key optical performance metrics of lasing media are the threshold carrier density, intrinsic and net optical gain, and the carrier recombination lifetime. Accurate estimation of these metrics is essential to make an informed selection of the gain medium in a laser. These metrics are usually determined using optical characterization techniques. Generally, it is desirable for a lasing medium to possess a low threshold carrier density. A lower threshold carrier density concurrently leads to a lower optical pump fluence/current density necessary to observe lasing in a laser diode. A high optical intrinsic gain and stronger mode confinement are desired to enable the material to overcome absorption losses from surrounding layers with minimal increase in the pump fluence/current. The population of photons and carriers in a laser diode are modeled using rate equations, which require information on the recombination rates.[21] The relationships between the gain, relaxation lifetime, and carrier densities have been theoretically described and experimentally verified for III–V semiconductors. However, the carrier dynamics in perovskites, colloidal quantum dots, and organic semiconductors are different. While the interplay between the parameters has been studied in a few works,[22–24] they are not as well understood as III–V semiconductors.

In particular, the optically pumped ASE threshold fluence has been widely used to benchmark material films and stacks due to the relative ease of experimenting. While the threshold fluence of a material primarily depends on its radiative properties, there are other influential factors such as the film thickness, absorption coefficient,[16,25] pump source wavelength,[26] pump pulse duration,[27–29] and excitation area.[16,17,30–32] For an archetypical perovskite film like methylammonium iodide ($MAPbI_3$), the ASE threshold fluences in the literature vary across an order of magnitude[9] due to the contributions from these factors. Besides these aforementioned factors, the method of estimation of the threshold fluence can also impact the reported value.[33] This aspect is further explored in this work.

The commonly used pump excitation spots used to perform PL measurements have a circularly symmetric Gaussian

N. Annavarapu, I. Goldberg, K. Elkhouly, S. Hamdad, J. Genoe, P. Heremans
ESAT Department
KU Leuven
Kasteelpark Arenberg 10, 3001 Leuven, Belgium
E-mail: paul.heremans@imec.be

N. Annavarapu, I. Goldberg, K. Elkhouly, S. Hamdad, J. Genoe, R. Gehlhaar, P. Heremans
imec
Kapeldreef 75, 3001 Leuven, Belgium
E-mail: robert.gehlhaar@imec.be

The ORCID identification number(s) for the author(s) of this article can be found under https://doi.org/10.1002/adpr.202400065.

DOI: 10.1002/adpr.202400065

intensity distribution, corresponding to the TEM_{00} mode of the pump laser.[34] The average pump fluences are calculated by dividing the total energy per pulse or power by the area of the excitation. However, this approach can lead to improper estimation of the threshold fluence because the spatial intensity distribution of the excitation is neglected. In this work, we study the ASE emission in both spatial and spectral domains using different pump profiles. By analyzing the spatial PL spectra emitted by a lead-halide perovskite film at different pump powers, we establish that the threshold fluence is more accurately correlated with the peak fluence of the excitation, rather than the average fluence calculated over a beam area, the latter being most often used in literature. Subsequently, we provide an alternate expression for determining the average fluence of arbitrary beam shapes, along with simple conversions to calculate the peak fluence of two-dimensional (2D) Gaussian beams and one-dimensional (1D) stripes. Furthermore, our findings underscore the advantages of employing a uniform excitation profile, such as a 1D stripe or a flat-top profile, in the determination of optically pumped threshold fluence values.

2. Results and Discussion

For a circularly symmetric spot with a Gaussian intensity distribution, the average excitation fluence is calculated using Equation (1):

$$I_F(D_X) = \frac{E_p}{\text{Area}} = \frac{4E_p}{\pi D_X^2} \tag{1}$$

where E_p is the energy per pulse or the power of the source laser and D_X is the diameter of the beam. The diameter is typically measured between points where the intensity drops by a factor of e^{-2} compared to the peak, denoted as the 4σ diameter.[34] In some reports, the diameter is measured at the full width at half maximum (FWHM).[35,36]

Figure 1a shows a 2D intensity distribution of a Gaussian beam. The average fluence calculated using Equation (1) (assuming a 4σ diameter) ignores the intensity variation of the Gaussian beam. This produces a value that strongly underestimates the peak fluence, as shown in Figure 1b. The fluence distributions of the Gaussian and averaged beams (both for 4σ and FWHM areas) are compared along one axis in Figure 1c, and it is evident that the average fluence improperly estimates the true fluence impinged on the sample.

A laser beam, when impinged on a perovskite film, is absorbed to generate electron–hole pairs. In the case of perovskites, the generated carriers typically diffuse outward in distances ranging from hundreds of nanometers to a few microns,[37–39] before recombining through radiative and nonradiative decay processes. Therefore, an excitation spot size significantly larger than the diffusion length would produce a carrier density profile resembling the pump fluence distribution.[40] For the nonuniform illumination, at the threshold, the inversion carrier density is generated close to the peak in a relatively smaller area. As the total pump energy (power) increases, a wider area achieves inversion carrier density. Such behavior is demonstrated by analyzing the spatial PL distribution of an archetypical perovskite waveguide (≈120 nm-thick $MAPbI_3$ on glass covered by ≈100 nm PMMA) using an imaging spectroscopy setup (schematically shown in **Figure 2**a).

Since spontaneous emission intensity is linearly proportional to the pump fluence below the threshold, the excitation profile could be directly visualized by measuring the spatial PL intensity distribution. To exclude nonlinear ASE contribution, the diameter of the pump spot is estimated by imaging the PL at pump fluences sufficiently below the ASE threshold (Figure 2b). By fitting the intensity profile to a Gaussian distribution along each axis, the circular spot diameter can be estimated (Figure 2c,d). The maximum width of the entrance slit into the spectrometer truncates the circular PL image along the *x*-axis, as seen in Figure 2b,c.

The imaging spectrometer is capable of recording spectra while preserving spatial information along one axis. Therefore, the area emitting ASE can be monitored at different pump fluences. **Figure 3** shows the spatial PL spectra at three different pump fluences, namely, below the ASE threshold, at the threshold, and far above the threshold. Here, we define the "threshold condition" using the visual method described by Milanese et al.[33] where the fluence at which ASE emission is first detected in the PL spectrum is designated as the threshold fluence. As expected, ASE appears around the peak of the excitation profile close to the threshold and is emitted from a wider area upon pumping the sample with higher energies.

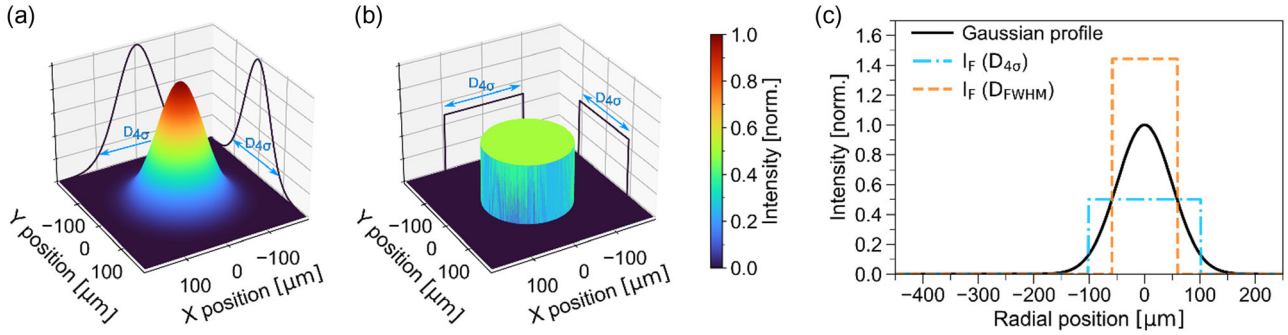

Figure 1. a) Illustration of the intensity distribution in a 2D circularly-symmetric Gaussian excitation spot and b) the average intensity distribution within the 4σ diameter on the same Z scale. c) Comparison of fluence distributions of the Gaussian beam (black, solid), the average in the 4σ diameter (blue, dash-dotted), and FWHM diameter (orange, dashed) along the radial axis.

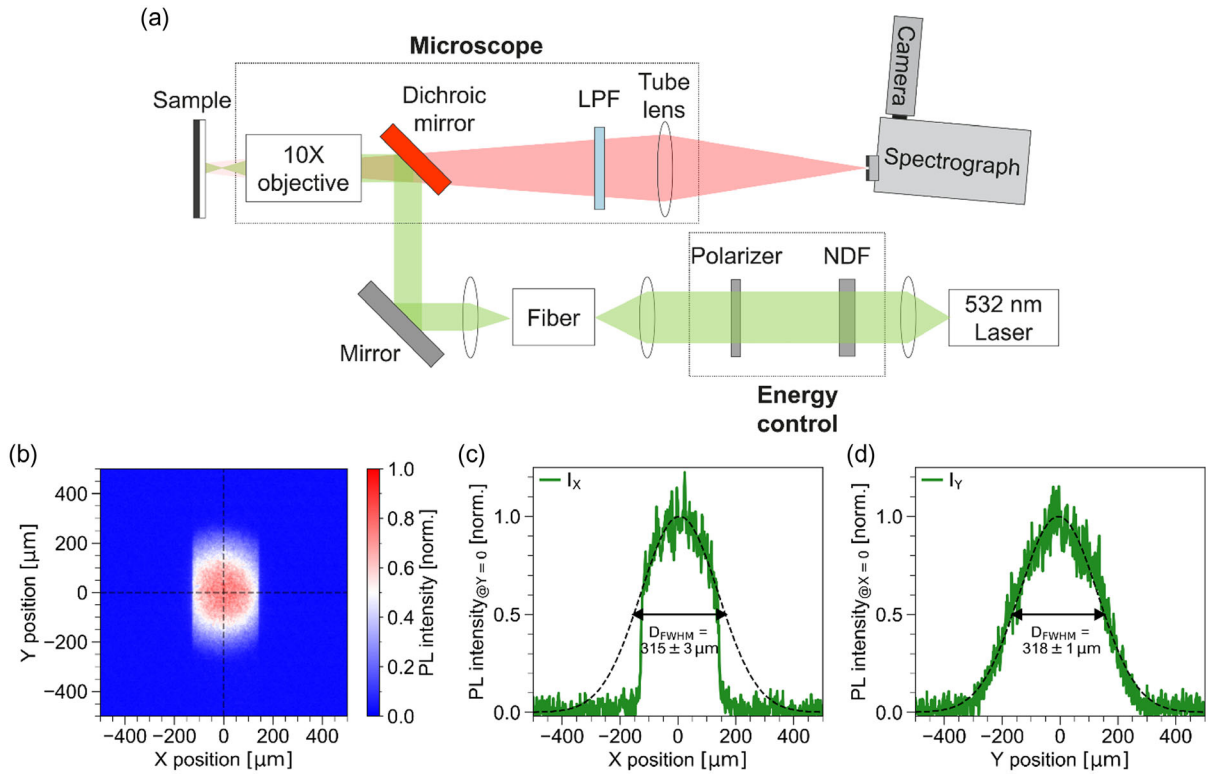

Figure 2. a) Schematic of optical setup used to perform confocal PL measurements using a Gaussian excitation spot. b) PL intensity distribution at pump energy below threshold (corresponding to a peak fluence, $I_{F,peak} = 20\ \mu J\ cm^{-2}$). The black dashed lines signify cut-lines along which the beam diameter is fit. c,d) PL intensity distribution along the *X*-axis (*Y*-axis) is fit to a Gaussian distribution (black).

Therefore, the peak excitation fluence at the threshold energy represents a realistic upper bound to the threshold fluence for a given experiment. The optical IO-curve obtained in this experiment is shown in Figure S1, Supporting Information, where the input fluence is represented by both the peak fluence and $I_F(D_{4\sigma})$.

The use of broader area approximations results in lower threshold fluence estimations, highlighting the importance of considering the pump profile. To correct for this in the case of a circular Gaussian beam, one could double the average fluence within the 4σ area. Alternatively, if the FWHM diameter is considered, a different factor must be used to estimate the peak fluence.

$$I_{F,peak} = 2 \cdot I_F(D_{4\sigma}) \approx 0.693 \cdot I_F(D_{FWHM}) \quad (2)$$

A general formula to estimate the average fluence for any arbitrary beam shape is given below:

$$I_{F,avg} = \frac{\iint_{Area} I(x,y)\,dx\,dy}{\iint_{Area} dx\,dy} \quad (3)$$

where $I(x,y)$ denotes the in-plane distribution of intensity of the pump beam. This equation is very similar to Equation (1) where the pump energy (power) is divided by an area of interest, such as the area within the FWHM diameter of a Gaussian distribution. However, instead of relying on the total pump energy (power), the energy (power) contained within the area of interest is explicitly calculated. This approach eliminates the possibility of estimating the average fluence higher than the peak fluence. By choosing a narrow area of interest centered around the peak of the intensity distribution, the peak fluence can be estimated. This concept is illustrated in Figure S2, Supporting Information, where the updated average fluences within the 4σ, FWHM, and a narrower diameter are shown for the same Gaussian beam as the one shown in Figure 1a,c.

While a Gaussian excitation provides the simplest experiment to measure the ASE threshold, it comes at a cost. As shown in Figure 3, the area that emits ASE changes dynamically with the pump energy, which implies that the inversion volume changes during the experiment. It has been shown in multiple reports that the ASE threshold of any medium is inversely proportional to the size of the excitation.[16,17,30–32] This threshold reduction is attributed to the increased guided photon's interaction length with the gain medium, which increases the probability of stimulated emission despite maintaining the same carrier inversion density.[32] Therefore, the same material characterized using two different Gaussian excitation diameters would yield different ASE thresholds, which complicates the comparison of thresholds across different works.

To avoid the dynamic change in inversion volume, we advocate for a flat-top excitation profile or alternatively a narrow, stripe-shaped excitation. Shaping the laser beam into a stripe with a uniform pump intensity along one axis is relatively simple. The pump laser beam must be expanded, focused along one axis using a cylindrical lens, and passed through a mechanical slit. If the expanded beam exceeds the mechanical slit opening, a

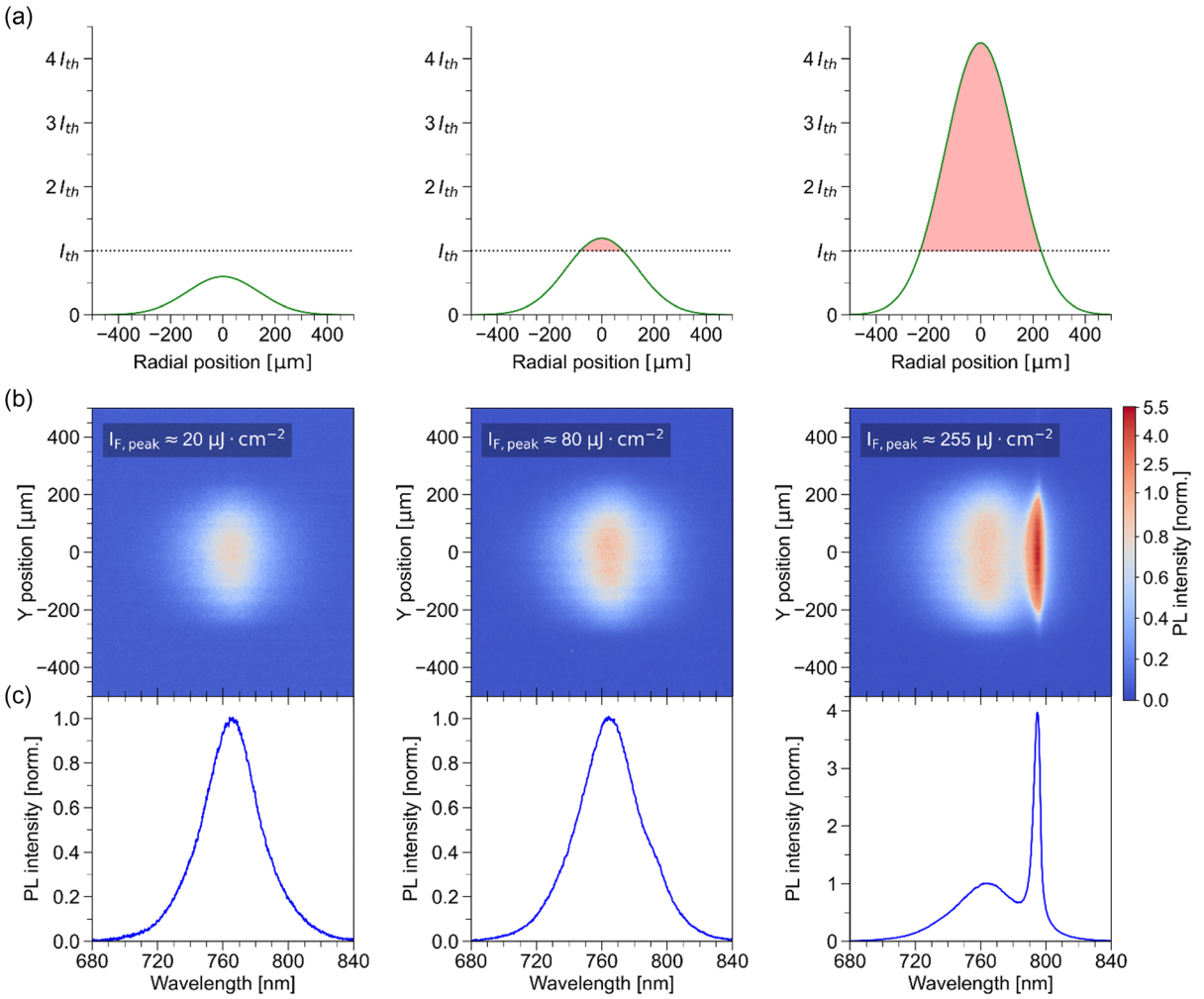

Figure 3. a) Illustrations of Gaussian excitation intensity along the radial axis with respect to threshold fluence. Red-shaded zone represents inverted volume. b) Spatial PL spectra and c) binned PL spectra measured at different input peak fluences of a 2D Gaussian beam profile. All spectra are normalized to the peak of the spontaneous emission spectrum. I_{th} denotes a "true" ASE threshold.

relatively uniform beam is obtained at the exit of the slit. However, excessive beam expansion can result in a loss of optical power, making it difficult to excite ASE or lasing. Therefore, the setup must be adjusted to create an expanded beam that ensures uniform gain along the stripe while also allowing the excitation of ASE or lasing at fluences higher than the threshold. An intensity drop of up to 10% at the ends of the stripe is adequate to ensure uniform gain along the stripe,[41] and therefore would not compromise threshold measurements.

Similar to the circular excitation, this beam shape also permits an increase in the inversion volume during the threshold measurement experiment. However, the change in inversion volume is mainly limited to one (lateral) axis, which is much smaller than the longitudinal axis. In such a case, increasing the pump power does not significantly increase the interaction length of the guided photon with the medium. **Figure 4** compares the near-field spectra of the sample at different pump fluences using a stripe-shaped excitation. The setup used for this experiment is the same as the one used in reference,[42] and the excitation profile is shown in Figure S3, Supporting Information. The corresponding optical IO curve for the experiment is shown in Figure S4, Supporting Information.

The ASE intensity along the stripe length is extracted by integrating the total intensity at each position and subtracting the spontaneous emission contribution.[42] At pump fluences in the vicinity of the threshold fluence, ASE is emitted uniformly along the stripe, shown in Figure S5, Supporting Information. At higher fluences, the ASE intensity behaves differently compared to the Gaussian profile. The ASE intensity reaches a maximum at the ends of the stripe, which is attributed to guided mode amplification[42] in a medium with uniform gain and low backscattering. Simple expressions for estimation of the peak fluence of a stripe excitation are given below:

$$I_{\mathrm{F}}(W_X) = \frac{E_{\mathrm{p}}}{\mathrm{Area}} = \frac{E_{\mathrm{p}}}{L \cdot W_X} \tag{4}$$

$$I_{\mathrm{F,peak}} \approx 1.59 \cdot I_{\mathrm{F}}(W_{4\sigma}) \approx 0.94 \cdot I_{\mathrm{F}}(W_{\mathrm{FWHM}}) \tag{5}$$

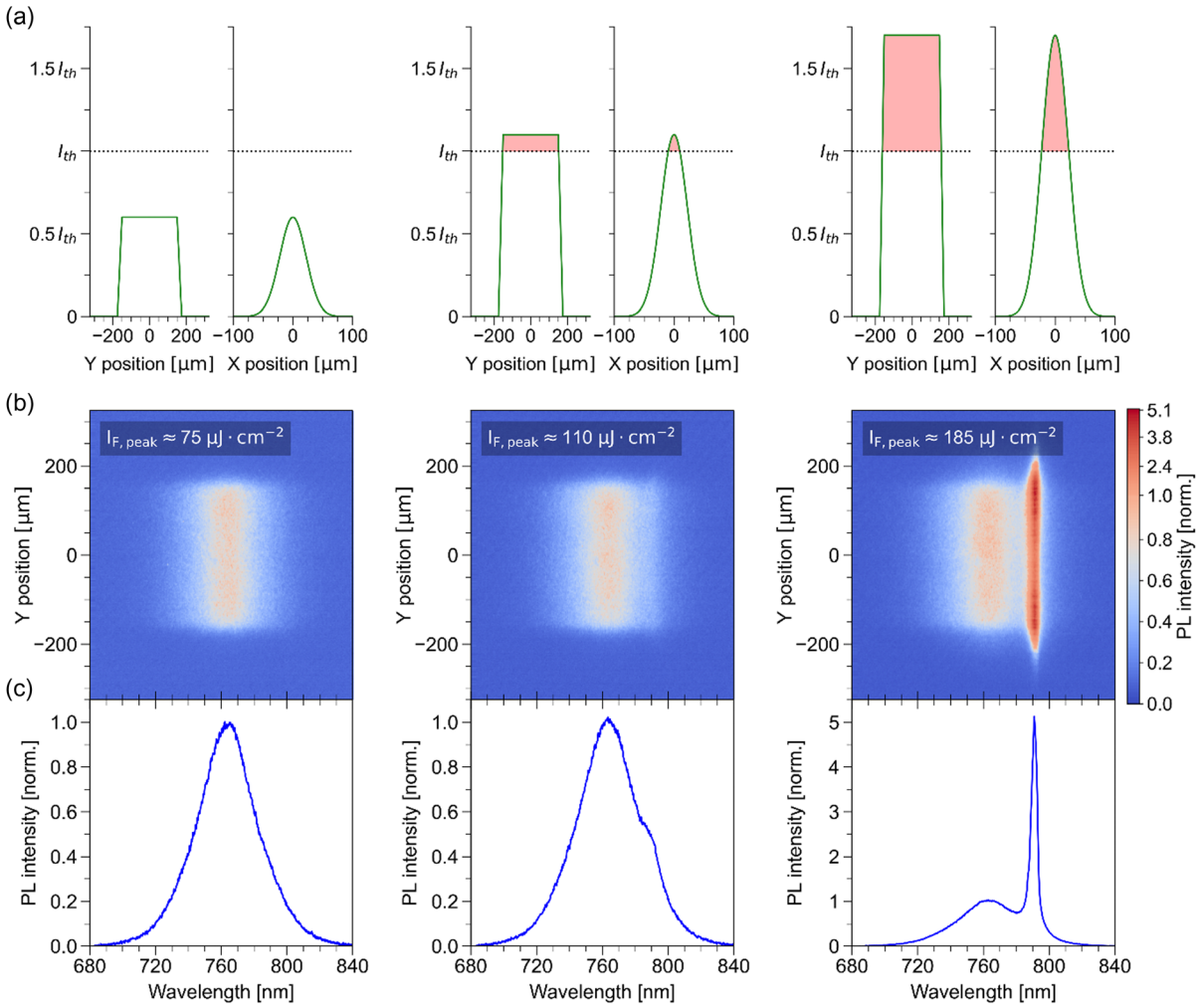

Figure 4. a) Illustrations of excitation stripe intensity with respect to threshold fluence. The red-shaded zone represents inverted volume. b) Spatial PL spectra and c) binned PL spectra measured at different input peak fluences of a stripe-shaped excitation. All spectra are normalized to the peak of the spontaneous emission spectrum.

where L depicts the length of the stripe along the peak fluence isoline and W_X describes the width of the transverse Gaussian profile. The peak fluence conversions were provided for Gaussian profile width measured in FWHM and 4σ.

Using a flat-top excitation or a uniform stripe excitation ensures that the photoexcited carrier density is constant across the excited area, which permits a more exact estimation of the threshold fluence and threshold carrier densities. Since the threshold fluence depends on the excitation size, a proper comparison of the threshold fluences between different experiments can only be performed when the excitation intensity profiles are similar. Therefore, we encourage researchers to provide detailed information on the excitation profile and the protocol used to extract the ASE threshold fluence in their PL measurements.

3. Conclusion

In this work, we have proven experimentally that the ASE threshold fluence estimation for lasing media corresponds to the peak fluence of the excitation, rather than the average measured across a fixed diameter. Using a circular Gaussian excitation spot, we show that the average fluence calculated in the 4σ diameter underestimates the true threshold fluence by a factor of two. We also show how the area emitting ASE (corresponding to the inversion volume) increases during the experiment when higher pump powers are applied. This is not ideal since the inversion volume directly influences the ASE threshold. To address these issues, we recommend using a flat-top or uniform stripe excitation. This configuration provides a threshold fluence value that is less sensitive to the input pump intensity distribution. We provided a general formula to calculate the peak fluence for an arbitrary beam profile. Furthermore, we provided simple conversions of average fluences to peak fluences for 2D Gaussian and stripe excitation profiles. Estimating the peak fluence provides an upper bound to the threshold fluence (and carrier density) for a given excitation geometry. Rigorous comparisons of optical thresholds can be performed across different films if the peak fluences are compared using similar pump parameters, such

as the wavelength, excitation shape, and pulse duration. To facilitate that, we encourage researchers to report their excitation beam characterization and threshold estimation procedures.

4. Experimental Section

Sample Preparation: An equimolar mixture of perovskite precursor salts, MAI (CH_3NH_3I) and PbI_2, was dissolved in the N,N-dimethylformamide (DMF) to obtain 1.2M solution. The dilution was later adjusted to obtain 120 nm thick $MAPbI_3$ films by a one-step spin-coating. $MAPbI_3$ precursor solution was spin-coated at 6000 rpm for 34 s and the wet film was quenched by dropping 150 µL of toluene four seconds after the start of the spinning. The film was annealed at 70 °C for five minutes. To protect the film from degradation during ambient optical measurement, polymethyl methacrylate (PMMA) (40 mg mL^{-1} in chlorobenzene) was spin-coated above the perovskite at 4000 rpm for 60 s without sequential annealing.

The films were fabricated on Si/SiO_2 substrates which were cleaved to produce a uniform-thickness waveguide with a smooth edge. The thickness of the thermal SiO_2 was around 1000 nm to isolate the perovskite mode from the substrate.

Optical Characterization: A diode-pumped Q-switched laser (CryLaS FTSS355-300) with a pulse duration of ≈2.3 ns (measured temporally in FWHM) is used to excite our sample for the PL measurements. The pulse energy is modulated using a combination of neutral density filters and a polarizer. Laser pulses are focused into a fiber which permits relocation of the beam to other locations on the optical table. The light from the fiber is collected using a defocused lens, which produces a mildly diverging beam. This beam is passed into the exit aperture of the microscope objective through a dichroic mirror, and produces a Gaussian excitation profile at the focal plane of the microscope. The diameter of the Gaussian excitation can be tuned by adjusting the divergence of the beam. PL emitted from a 2-D excitation spot is collected using the microscope objective, transmitted through the dichroic mirror, and subsequently focused on the entrance slit of the imaging spectrometer using a tube lens.

Supporting Information

Supporting Information is available from the Wiley Online Library or from the author.

Acknowledgements

The authors acknowledge funding from the European Research Council under the European Horizon 2020 Programme/ERC grant agreement no. 835133 (ULTRA-LUX).

Conflict of Interest

The authors declare no conflict of interest.

Data Availability Statement

The data that support the findings of this study are available from the corresponding author upon reasonable request.

Keywords

beam characterization, lasing threshold, peak fluence estimation, perovskites, threshold fluences

Received: April 11, 2024
Revised: July 18, 2024
Published online: August 5, 2024

[1] L. N. Quan, B. P. Rand, R. H. Friend, S. G. Mhaisalkar, T.-W. Lee, E. H. Sargent, *Chem. Rev.* **2019**, *119*, 7444.
[2] N. Tessler, *Adv. Mater.* **1999**, *11*, 363.
[3] Y.-S. Park, J. Roh, B. T. Diroll, R. D. Schaller, V. I. Klimov, *Nat. Rev. Mater.* **2021**, *6*, 382.
[4] A. Zampetti, A. Minotto, F. Cacialli, *Adv. Funct. Mater.* **2019**, *29*, 1807623.
[5] A. Fakharuddin, U. Shabbir, W. Qiu, T. Iqbal, M. Sultan, P. Heremans, L. Schmidt-Mende, *Adv. Mater.* **2019**, *31*, 1807095.
[6] Y. Shirasaki, G. J. Supran, M. G. Bawendi, V. Bulović, *Nat. Photonics* **2013**, *7*, 13.
[7] M. L. De Giorgi, M. Anni, *Appl. Sci.* **2019**, *9*, 4591.
[8] Q. Zhang, Q. Shang, R. Su, T. T. H. Do, Q. Xiong, *Nano Lett.* **2021**, *21*, 1903.
[9] A. Liu, G. Guan, X. Chai, N. Feng, M. Lu, X. Bai, Y. Zhang, *Laser Photonics Rev.* **2022**, *16*, 2200189.
[10] N. Feng, M. Lu, S. Sun, A. Liu, X. Chai, X. Bai, J. Hu, Y. Zhang, *Laser Photonics Rev.* **2023**, *17*, 2200908.
[11] B. Li, T. Zhou, X. Fang, W. Zhang, X. Li, Z. Guan, J. Li, L. Wang, S. Hark, Z. Zhang, *J. Mater. Chem. C* **2019**, *7*, 4102.
[12] X. Wang, M. Shoaib, X. Wang, X. Zhang, M. He, Z. Luo, W. Zheng, H. Li, T. Yang, X. Zhu, L. Ma, A. Pan, *ACS Nano* **2018**, *12*, 6170.
[13] P. J. Cegielski, A. L. Giesecke, S. Neutzner, C. Porschatis, M. Gandini, D. Schall, C. A. R. Perini, J. Bolten, S. Suckow, S. Kataria, B. Chmielak, T. Wahlbrink, A. Petrozza, M. C. Lemme, *Nano Lett.* **2018**, *18*, 6915.
[14] S. Wang, Y. Liu, G. Li, J. Zhang, N. Zhang, S. Xiao, Q. Song, *Adv. Opt. Mater.* **2018**, *6*, 1701266.
[15] H. Kim, K. Roh, J. P. Murphy, L. Zhao, W. B. Gunnarsson, E. Longhi, S. Barlow, S. R. Marder, B. P. Rand, N. C. Giebink, *Adv. Opt. Mater.* **2020**, *8*, 1901297.
[16] N. Annavarapu, I. Goldberg, S. Hamdad, K. Elkhouly, R. Puybaret, D. Sabuncuoglu Tezcan, J. Genoe, R. Gehlhaar, P. Heremans, *Adv. Opt. Mater.* **2024**, *12*, 2302496.
[17] K. Elkhouly, I. Goldberg, X. Zhang, N. Annavarapu, S. Ham, dad, G. Croes, C. Rolin, J. Genoe, W. Qiu, R. Gehlhaar, P. Heremans, *Nat. Photonics* **2024**, *18*, 132.
[18] N. Ahn, C. Livache, V. Pinchetti, H. Jung, H. Jin, D. Hahm, Y.-S. Park, V. I. Klimov, *Nature* **2023**, *617*, 79.
[19] K. Yoshida, J. Gong, A. L. Kanibolotsky, P. J. Skabara, G. A. Turnbull, I. D. W. Samuel, *Nature* **2023**, *621*, 746.
[20] A. S. D. Sandanayaka, T. Matsushima, F. Bencheikh, S. Terakawa, W. J. Potscavage, C. Qin, T. Fujihara, K. Goushi, J.-C. Ribierre, C. Adachi, *Appl. Phys. Express* **2019**, *12*, 061010.
[21] B. E. A. Saleh, M. C. Teich, *Fundamentals of Photonics*, Wiley-Interscience, Hoboken, NJ **2001**.
[22] I. Suárez, E. J. Juárez-Pérez, V. S. Chirvony, I. Mora-Seró, J. P. Martínez-Pastor, *Phys. Rev. Appl.* **2020**, *13*, 064071.
[23] H. Jung, N. Ahn, V. I. Klimov, *Nat. Photonics* **2021**, *15*, 643.
[24] V. G. Kozlov, G. Parthasarathy, P. E. Burrows, V. B. Khalfin, J. Wang, S. Y. Chou, S. R. Forrest, *IEEE J. Quantum Electron.* **2000**, *36*, 18.
[25] M. Anni, A. Perulli, G. Monti, *J. Appl. Phys.* **2012**, *111*, 093109.
[26] J. Qin, Y. Tang, J. Zhang, T. Shen, M. Karlsson, T. Zhang, W. Cai, L. Shi, W.-X. Ni, F. Gao, *Mater. Horiz.* **2023**, *10*, 1446.
[27] N. Pourdavoud, T. Haeger, A. Mayer, P. J. Cegielski, A. L. Giesecke, R. Heiderhoff, S. Olthof, S. Zaefferer, I. Shutsko, A. Henkel, D. Becker-Koch, M. Stein, M. Cehovski, O. Charfi, H. Johannes, D. Rogalla, M. C. Lemme, M. Koch, Y. Vaynzof, K. Meerholz,

W. Kowalsky, H. Scheer, P. Görrn, T. Riedl, *Adv. Mater.* **2019**, *31*, 1903717.
[28] C.-Y. Huang, C. Zou, C. Mao, K. L. Corp, Y.-C. Yao, Y.-J. Lee, C. W. Schlenker, A. K. Y. Jen, L. Y. Lin, *ACS Photonics* **2017**, *4*, 2281.
[29] G. L. Whitworth, J. R. Harwell, D. N. Miller, G. J. Hedley, W. Zhang, H. J. Snaith, G. A. Turnbull, I. D. W. Samuel, *Opt. Express* **2016**, *24*, 23677.
[30] C. Cho, T. Antrack, M. Kroll, Q. An, T. R. Bärschneider, A. Fischer, S. Meister, Y. Vaynzof, K. Leo, *Adv. Sci.* **2021**, *8*, 2101663.
[31] K. N. Bourdakos, L. A. Cury, A. P. Monkman, *Org. Electron.* **2011**, *12*, 1142.
[32] G. I. Peters, L. Allen, *J. Phys. A: Gen. Phys.* **1971**, *4*, 238.
[33] S. Milanese, M. L. De Giorgi, L. Cerdán, M.-G. La-Placa, N. F. Jamaludin, A. Bruno, H. J. Bolink, M. V. Kovalenko, M. Anni, *Molecules* **2022**, *27*, 4261.
[34] O. Svelto, *Principles of Lasers*, Springer US, Boston, MA **2010**.
[35] V. S. Chirvony, I. Suárez, J. Sanchez-Diaz, R. S. Sánchez, J. Rodríguez-Romero, I. Mora-Seró, J. P. Martínez-Pastor, *Adv. Mater.* **2023**, *35*, 2208293.
[36] S. Yakunin, L. Protesescu, F. Krieg, M. I. Bodnarchuk, G. Nedelcu, M. Humer, G. De Luca, M. Fiebig, W. Heiss, M. V. Kovalenko, *Nat. Commun.* **2015**, *6*, 8056.
[37] Y. Zhao, A. M. Nardes, K. Zhu, *J. Phys. Chem. Lett.* **2014**, *5*, 490.
[38] W. Rehman, R. L. Milot, G. E. Eperon, C. Wehrenfennig, J. L. Boland, H. J. Snaith, M. B. Johnston, L. M. Herz, *Adv. Mater.* **2015**, *27*, 7938.
[39] Y. Li, W. Yan, Y. Li, S. Wang, W. Wang, Z. Bian, L. Xiao, Q. Gong, *Sci. Rep.* **2015**, *5*, 14485.
[40] A. Sridharan, N. K. Noel, B. P. Rand, S. Kéna-Cohen, *J. Phys. Chem. C* **2021**, *125*, 2240.
[41] A. L. Alvarado-Leaños, D. Cortecchia, G. Folpini, A. R. Srimath Kandada, A. Petrozza, *Adv. Opt. Mater.* **2021**, *9*, 2001773.
[42] N. Annavarapu, I. Goldberg, A. Papadopoulou, K. Elkhouly, J. Genoe, R. Gehlhaar, P. Heremans, *ACS Photonics* **2023**, *10*, 1583.